INTER AND INTRA-DIURNAL VARIATIONS OF CLOUDINESS OVER AFRICA FROM METEOSAT OBSERVATIONS

J. Ph. Duvel
and
L. A. Toledo Machado

Laboratoire de Météorologie Dynamique du C.N.R.S.
Ecole Polytechnique, F-91128 Palaiseau Cedex, France.

1. INTRODUCTION

The study of intraseasonal fluctuations of the convection, even at short time scale, may be an important source of information for the validation of the cloud parametrization in general circulation models (GCM). If GCMs are to represent mean states correctly, they should also describe the fluctuations related to physical processes governing the formation of the deep convection. Such a description is needed not only for the good representation of the present climate but also to increase the credibility of sensitivity studies. The aim of this study is to investigate the temporal variability and the related spatial structure of high and mid-level cloudiness over Africa and the neighbouring Atlantic ocean. We attempt to extract general characteristics suitable for GCM validation and improvement. Regional experiments, such as GATE, gave detailed information only for relatively small regions and for a relatively short period of time. Although satellite data are deficient in describing in sufficient detail atmospheric conditions associated with cloudiness, homogeneous satellite data give the opportunity to study spatial and temporal characteristics of the convection for larger regions and for longer time period than conventional data.

Part of the results presented in this paper - about the diurnal variation and the relation between convection and easterly waves - is a summary of the results presented in Duvel (1989, 1990). New results also are reported about the spatial structure of the convection and its fluctuations, the moisture budget associated with easterly waves and the inter-diurnal fluctuation of the convection over Central Africa.

2. DATA

We use three-hourly sampling of IR window (10.5-12.5 μm) Meteosat ISCCP B2 data for summers (June to September) 1983-88. In order to have a better comparison over the six years we applied the ESOC MIEC (Jones and Morgan, 1981) adjustment which gives an estimate of the IR radiance and brightness temperature as a function of the raw IR counts (0-255). Table I gives equivalences between this IR radiance, the brightness temperature and the corresponding altitude of emission computed using the LOWTRAN (Kneizys et al., 1983) transfer model with a standard tropical atmosphere. The area of investigation is the large area between 25° N and 5° S and 50° W and 50° E (fig.1). This area is divided into 533 regions of 2.5° x 2.5°. Since ISCCP B2 data is a sampling of the initial image (1 pixel of 6 both horizontally and vertically), each region contains roughly from 40 sampled pixels at the corners to 110 sampled pixels at the subsatellite point. The study is performed on the 976 available observations between 31 May (2330 GMT) and 30 September (2330 GMT) with

8 measurements per day. Wind fields come from analysed fields of the ECMWF (Lorenc, 1981; Bengtsson, 1985) at 1200 GMT and 0 GMT for the same 533 regions of 2.5° and for the 3 periods of 4 months.

In order to show in detail the response of cloudiness to different forcing, we draw the composite diurnal or wave evolution of the histograms over selected nearly homogeneous regions (Albright et al., 1985; Duvel and Kandel, 1985). Histograms are obtained for the period 10 June - 20 September of each year. The radiance interval is 0.25 $Wm^{-2}sr^{-1}$ and the surface percentage is then the number of pixels emitting in this radiance interval expressed as a percentage of the total number of pixel of the considered region. Note that histogram evolution figures must not be interpreted in terms of multi-layered clouds but in terms of clouds at different altitudes distributed over the whole considered area and with varying coverage from one day to another. The diurnal evolution of the population of each radiance level may then be interpreted - independently of other radiance levels - as the diurnal modulation of the probability of presence of clouds with top emitting this radiance. The coherence of their shape suggests however that histogram evolutions are in some cases representative of the effective diurnal behavior of a given cloud type (for example high convective cloud for lowest radiance levels).

TABLE 1. Equivalence between the filtered radiance (R) of the IR signal of Meteosat and the corresponding EBBT, altitude of the top of the cloud and pressure levels. P and z are estimated using the LOWTRAN radiative transfer model with the standard tropical atmosphere.

R ($Wm^{-2}sr^{-1}$)	EBBT (K)	z (km)	P (mb)
1	207	14.7	139
2	233	10.8	255
3	252	8.1	373
4	267	5.5	525
5	280	3.1	707

We also define cloud cover at two levels by thresholds in the IR radiance values. These thresholds have been determined using the histogram evolution technique and plotting the mean diurnal variation over large regions of Africa and Atlantic Ocean. The threshold selection depends on the population of the radiance levels (i.e. peak on the histograms) and on the coherence of the diurnal phase. For high level cloud (noted HI), we consider all pixels having a brightness temperature (or EBBT) lower than 253K (cloud top around 8km on the basis of the tropical model of LOWTRAN; IR radiance 3 Wm^{-2} sr^{-1}). This threshold corresponds to that used by Augustine (1984) to infer rainfall activity over the Pacific Ocean. For high and mid-level cloud (noted CL) we consider pixels with brightness temperature smaller than 276.5K (≈4km; IR radiance 4.75 Wm^{-2} sr^{-1}). The cloud amount in each 2.5° x 2.5° region is defined as the number of selected pixels over the total number of pixels in the region.

3. DIURNAL VARIATIONS

3. 1 Diurnal variation of the cloud cover

The diurnal variation is defined here as the coherent diurnal variation obtained by computing the mean value of the considered quantity for each available hour. The phase of the diurnal variation is very sensitive to the threshold chosen in the IR radiances even

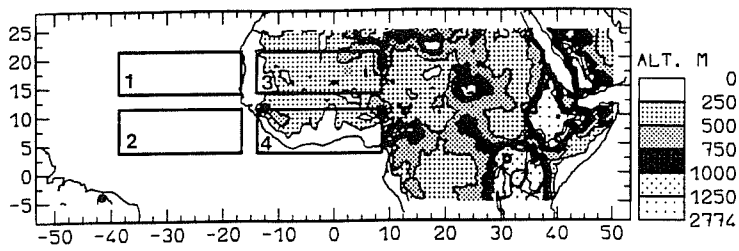

Fig.1: Orography of the studied regions based on a 1° resolution and definition of Regions 1-4.

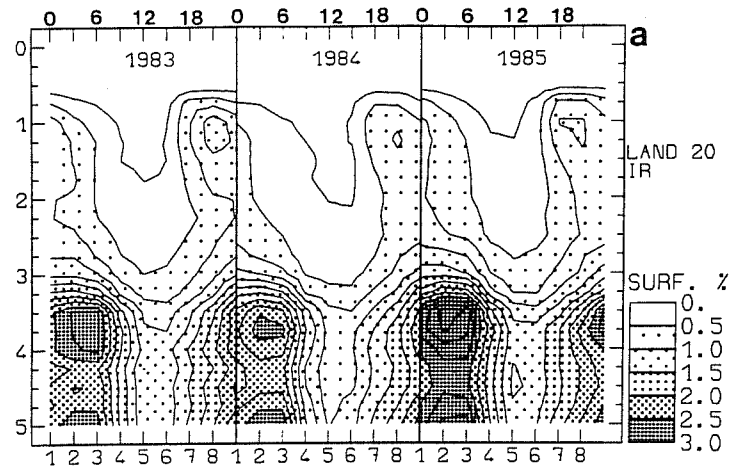

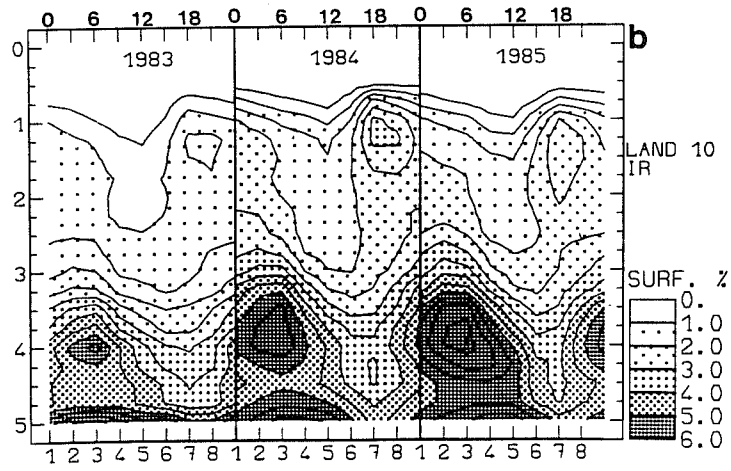

Fig.2: Diurnal histogram evolution for (a) region 3 and (b) region 4 on the average over each of the 3 summers. Abscissas are time with steps of 3 hours (the first being OO GMT) shown on the bottom and local time (LST) in hours on the top. Ordinates are radiance levels. Grey levels represent the surface covered by clouds with top emitting at the radiance level expressed as a percentage of the total surface of the region.

considering cloudiness with cloud top EBBT lower than 253K (Duvel, 1989). We show here only the diurnal histogram evolution which makes it possible to display the diurnal variation of the cloud cover at different radiance levels.

Over Saharo-Sahelian regions (region 3, see fig.1) and over the land part of active ITCZ (region 4), high and mid-level clouds appear to be concentrated mainly at 2 radiance levels around respectively 1.25 W $m^{-2}sr^{-1}$ (214 K) and 3.5 W $m^{-2}sr^{-1}$ (260K) (fig.2). Despite interannual changes in the fractional coverage, the diurnal behavior remains the same with a maximum high cloud coverage between 1800 and 2100 LST. Over region 3 (fig.2a), clouds at radiance levels between 3.5 and 4.5 W $m^{-2}sr^{-1}$ have a very strong diurnal modulation with maximum coverage between 0300 LST and 0600 LST and a rapid decrease until local noon. For regions further south (region 4) histogram evolution (fig.2b) shows that the morning dissipation of the high cloudiness is slower than for region 3. This is also true at lower levels where clouds persist until early afternoon over region 4 while they dissipate rapidly in the early morning over region 3. The importance of the diurnal solar forcing is then smaller than for the Saharo-Sahelian region 3. Note that this tendency also exists for low cloud in the Meteorological Office 5-layer general circulation model (Wilson and Mitchell, 1986). Most regions of Central Africa exhibit a diurnal behavior close to those of region 3 and 4 but, generally, with a larger amount of clouds and a larger diurnal modulation. Since the maximum deep convection occurs in the late afternoon over nearly all the African land regions, it is primarily the diurnal warming of the surface and of the lower troposphere which drives the diurnal cycle of the convection. The radiative effect described by Gray and Jacobson (1977) giving an early morning maximum due to different cooling rates at night between clusters and surrounding clear areas, has therefore little influence on the diurnal modulation of the convection over Africa.

For the oceanic regions, we present here only results for five 2.5° zonal bands between 2.5 and 12.5° N and extending from 27.5°W to 40°W. The 5 zonal bands are pointed out separately because the phase of the IR signal over the mid-Atlantic (not shown) has a latitudinal dependence with maximum development around 1600 LST at and north of 10° N and around 0400 LST around 5° N. This trend was previously pointed out by Murakami (1979). Histogram evolutions of the 5 zonal bands (fig.3) show however basically the same diurnal behavior. The latitudinal shift of the diurnal phase of high cloud over the mid-Atlantic is apparent only for the highest cloudiness. Diurnal behavior for radiance levels larger than 2.5 $Wm^{-2}sr^{-1}$ is practically the same for all latitudes. Even for the highest cloudiness, the different diurnal behaviors are related more to different populations of the radiance levels than to real differences in the shapes of the histogram evolution. The highest cloudiness (radiance 1 $Wm^{-2}sr^{-1}$) presents a very weak diurnal modulation with a slight maximum around 0400 LST. Clouds at lower levels (radiance between 1.5 and 2.-5 $Wm^{-2}sr^{-1}$) present however a stronger diurnal modulation with the largest concentration occurring between 1300 and 1600 LST. This shows that the maximum rainfall activity around 1500 LST found by Albright et al (1981) on the basis of GATE data may be extended westward to regions of the mid-Atlantic. There is a strong concentration of mid-level clouds having a maximum development before sunrise, i.e. slightly earlier than for land regions. The general shape of the diurnal variation is close to that found by Albright et al (1985) for the SPCZ-east (South Pacific Convergence Zone) region of the central Pacific Ocean and appears to be not only a characteristic of the Eastern Atlantic.

A striking result is the presence of a strong concentration of diurnally varying mid-level cloud over all studied regions of tropical Africa and Atlantic Ocean. Some pixels at

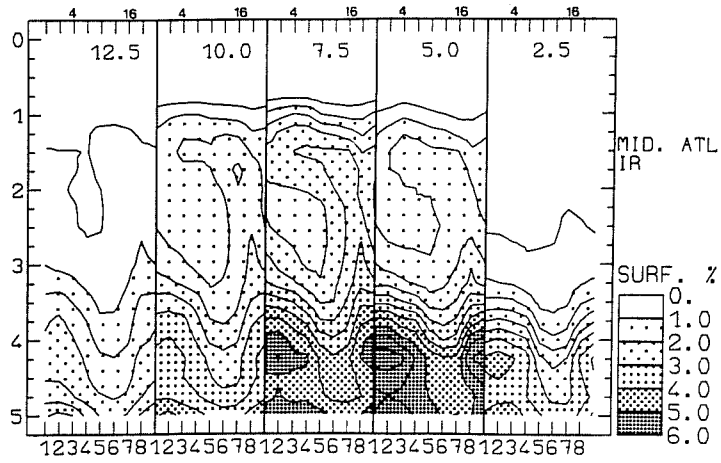

Fig.3: As in fig.2 but for the diurnal histogram evolutions on the average over the 3 summers for the region of the Mid-Atlantic. Results are presented on the average over each latitude band (from 2.5° N to 12.5° N with a step of 2.5°) between 27.5° W and 40° W.

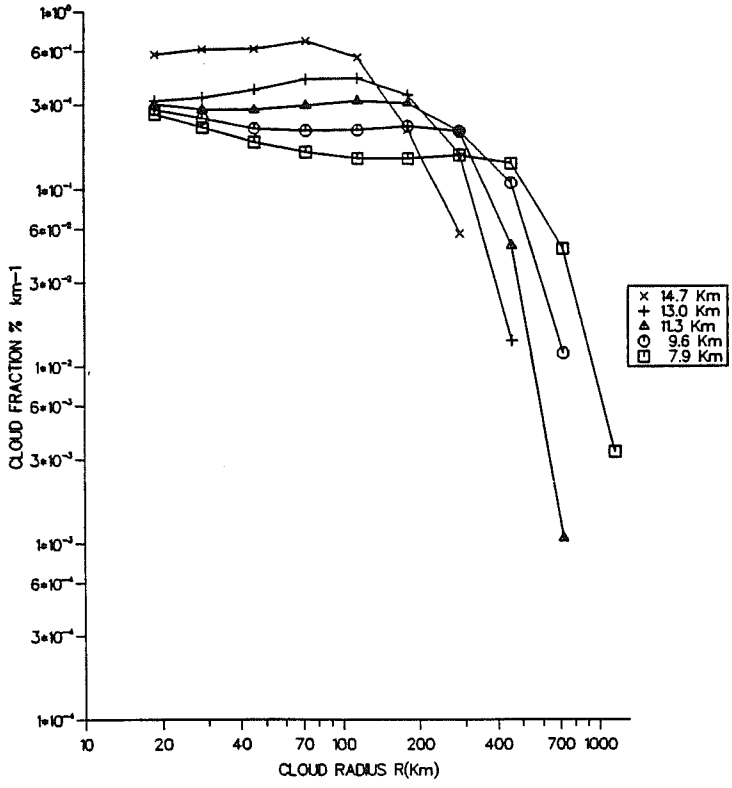

Fig.4: Cloud fraction density (eq.1) as a function of the cluster radius for different IR thresholds (from top to bottom: 207, 218, 230, 241 and 253 K).

these radiance levels may be covered by very thin or broken cirrus. However, since they are at higher altitude, a major contribution of cirrus at these radiance levels is unlikely because this would mean that their degree of "brokenness" or their IR transmittance (related to their thickness) are nearly constant over all regions for the 3 summers. These clouds, have a very stable diurnal phase with maximum coverage at sunrise. Previous results - over Brazil and West Africa in August and January 1979 (Duvel and Kandel, 1985) or for the GATE region in summer 1974 and central Pacific in winter 1979 (Albright et al., 1985) - also show the presence of this cloud type. This tends to show that these clouds are typical of tropical regions. The diurnal phase of these mid- level clouds enhances their planetary greenhouse effect at the expense of their planetary albedo effect. This diurnal behavior then contributes to the warming of the tropical regions. The nature and the origin of these mid-level clouds are however unclear. While the diurnal behavior is similar, the population of these radiance levels is certainly due to the presence of different type of clouds (i.e. altostratus, altocumulus, cumulus congestus), the proportion of each type of cloud varying with the atmospheric situation.

3. 1 Diurnal variation of the horizontal cloud structure

The spatial structure of the convection is computed on the basis of the infrared window images with the ISCCP-B2 sampling (a pixel of 5x5 km sampled every 30 km). The processing method we use is close to that of Wielicki and Welch (1986) and Welch et al (1988). However, the aim of the analysis is quite different since Welch et al, using visible imagery, try to isolate the cloud from the clear sky surrounding area, while, using infrared imagery, we attempt to define characteristic size of cloud clusters at different thresholds. A major hypothesis of our study is that the infrared threshold is related statistically to the cloud top altitude defining the cluster despite problems of semi-transparency or partially filled pixels. A cluster at a given threshold is defined as the surface covered by adjacent cloud cells having a top at or above the altitude corresponding to the threshold. Technically, we isolate groups of adjacent pixels with infrared value smaller or equal to the threshold. We then compute the surface of this cluster from which we deduce a radius assuming a circular shape centered on the center of mass of the surface.

Since the number of cluster decreases strongly with the size ($\approx R^{-2}$), in order to keep statistical significance, cluster classes are defined with a radius interval increasing with the radius as : $R_{c+1} = 1.58\ R_c$, where R_{c+1} and R_c are the boundaries of the cluster class c (constant interval $\Delta(\log(R))=0.2$). The smaller radius is considered to be 15 km so that the different classes are bounded by : 15, 24, 38, 60 km, etc... The cloud fraction density, previously used by Wielicki and Welch (1986) and Welch et al (1988) to characterize the distribution of the fraction covered by clouds (or clusters in our case) of different size, is defined as :

$$s(\Delta R) = \frac{1}{\Delta R.S_t} \sum_{r=R_c}^{R_{c+1}} N(r)\Pi r^2 \qquad (1)$$

where ΔR is the radius class interval, N(r) the number of clusters of radius r, S_t the total surface covered by clouds at the considered threshold. Note that with our definition of ΔR, if N(r) varies in $r^{-\alpha}$, both the surface density and the actual surface covered by clusters of radius R must vary in $R^{2-\alpha}$. In the same way, the cloud number density :

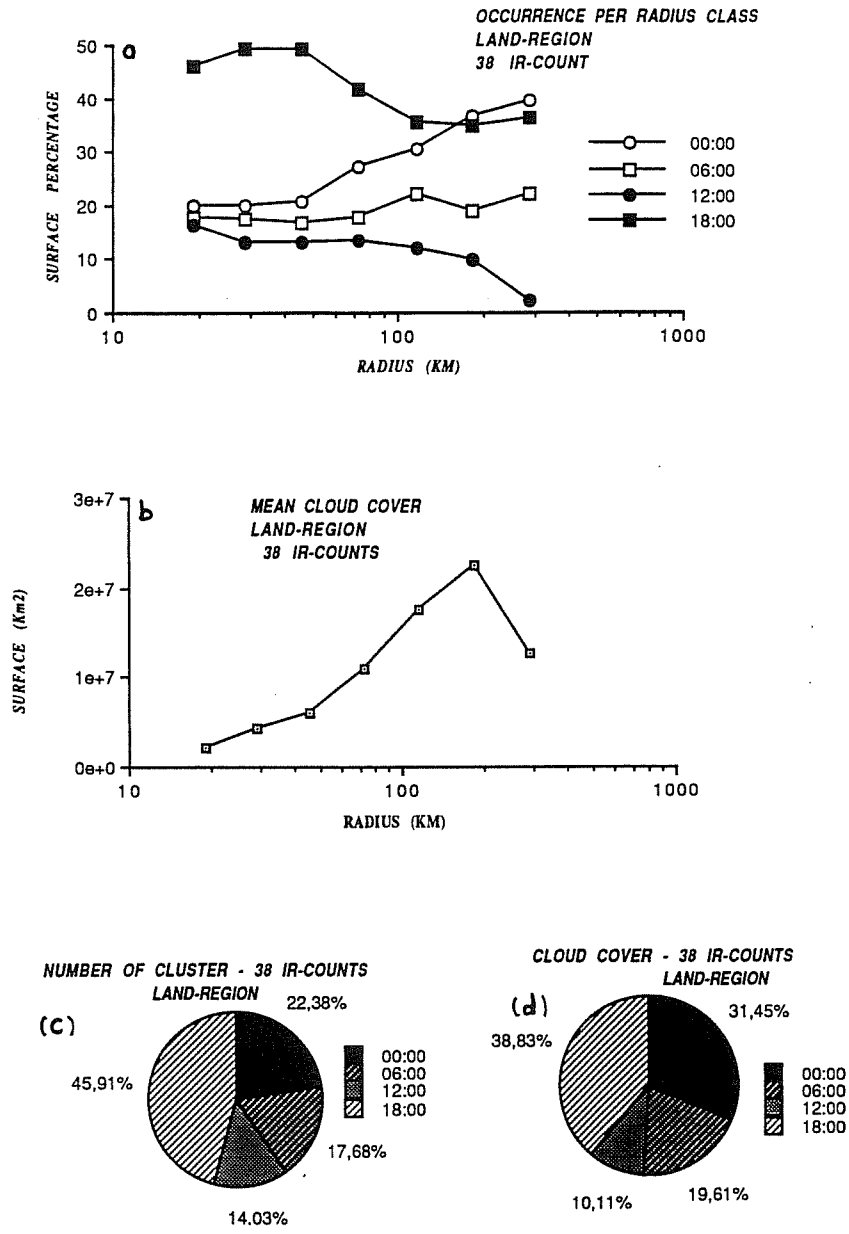

Fig.5: Statistic of the diurnal variation of clusters for land regions 3 and 4 for summer 1985 and for infrared threshold 218K (≈13km) (a) Cluster coverage at a given hour, expressed as a percentage of the mean coverage, for different cluster radius classes. (b) Mean surface coverage for the different cluster radius classes (c) Diurnal variation of the number of clusters. (d) Diurnal variation of the cloud cover.

$$n(\Delta R) = \frac{1}{\Delta R.S_t} \sum_{r=R_c}^{R_{c+1}} N(r) \quad , \qquad (2)$$

also defined by Wielicki and Welch (1986), must vary in $R^{-\alpha}$.

The mean cloud fraction density at midnight, for the whole region (fig.1) and 6 summers (JJA, 83 to 88), is reported in figure 4 for different infrared thresholds. The shape of these curves is similar for all thresholds, the fraction density remaining nearly constant until a point from which it decreases strongly. This "break point" occurs for larger clusters as the altitude decreases and corresponds to weak occurrence of the largest clusters despite the larger radius interval considered. Before the "break point", all cluster size are present on nearly all images, while, for cluster size larger than the "break point" radius, the probability of presence becomes weak. There are two main characteristics : first, the cluster size distribution is similar at all thresholds, the only strong difference being the larger occurrence of large clusters as the altitude (infrared threshold) decreases (increases). Second, there is no preferential cluster size, but the number of clusters decreases roughly as the square of the radius giving a nearly equal contribution of clusters at any size to the total cloud cover. A study now in progress shows that these characteristics are conserved while considering smaller regions, shorter time period (even a single day for large regions) and other infrared thresholds. Obviously, for small regions, one must consider long time period to agree with these statistics. The fact that the slope of the cluster size distribution before the "break point" is weak and increases slightly from high to lower levels (except the highest level at 14.7 km) is not yet understood.

The diurnal modulation of the spatial structure of the cloud clusters, at the "level" 13 km (EBBT≈220 K) and for JJAS 1985, is displayed on figure 5. For land regions of West Africa (regions 3 and 4 on fig.1), the number of high clusters (>13 km) and the surface covered by these clusters (fig 5c and 5d) present both a strong diurnal modulation with a large maximum at 1800 L.T. and a sharp minimum at noon. The diurnal modulation of the cluster size distribution (fig. 5a) is presented as the hourly deviation of the surface covered by clusters in a radius class expressed as a percentage of the mean cloud cover in this class. There is a dramatic increase of the surface covered by all cluster sizes between noon and 1800 L.T., with a relatively larger variation for small clusters. Between the end of the afternoon and midnight, only the surface covered by the largest clusters (R>150 km) continue to increase. At the same time, the surface covered by small clusters (R<70 km) decreases rapidly to a value which remains nearly constant for the rest of the day. Between midnight and noon, the covered surface decreases progressively with a larger amplitude for large clusters. Note that, because of the increasing radius interval with size, the weight of large clusters in fig.5a is larger (fig.5b).

For oceanic regions (regions 1 and 2), the diurnal variation of the number of clusters (fig. 6c) is not significant. The cloud cover (fig. 6d) presents however a small diurnal variation with maximum coverage at 0600 L.T. and noon. This diurnal variation is mainly due to clusters with radius larger than roughly 100 km (fig. 6a). This result is interesting because it is in agreement with the hypothesis of Gray and Jacobson (1977) diagnosing a significant radiative effect on the diurnal variation only for large clusters. Crude estimate of this radiatively induced increase of the convection, generated by difference in the cooling rate at night between the cluster and its relatively clear environment, predicts a maximum strengthening of the convergence in early morning.

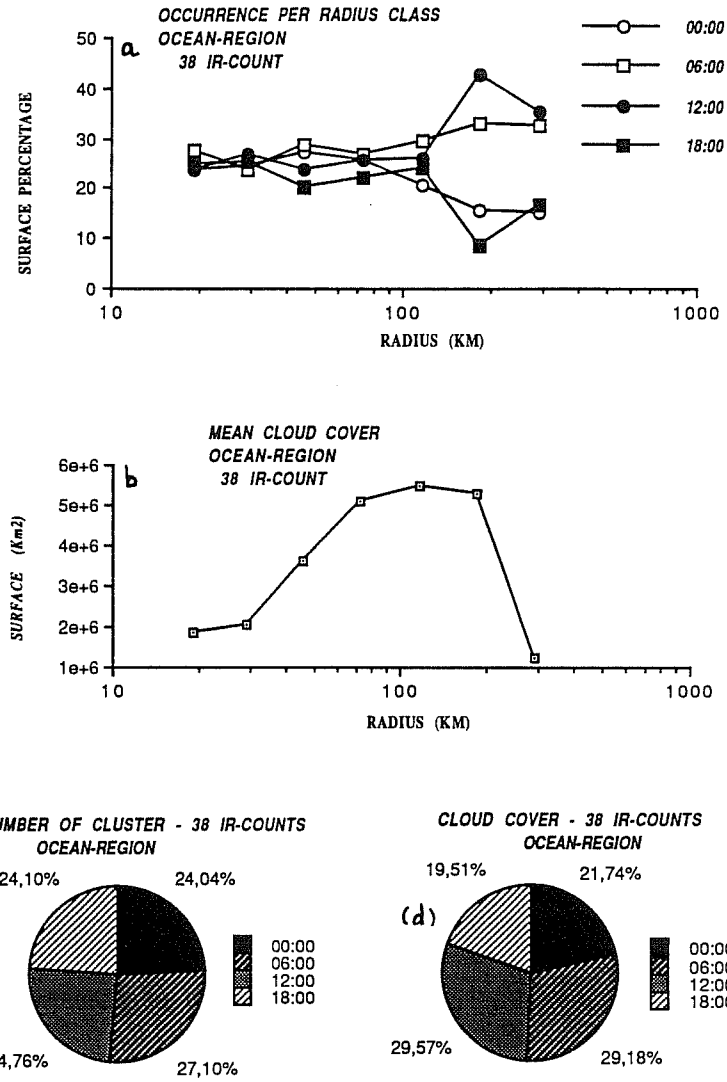

Fig.6: As in fig.5 but for ocean regions 1 and 2.

However, as noted by Gray and Jacobson, a considerable lag in response is to be expected in most cases, depending on the atmospheric state in which the disturbance is embedded. The maximum horizontal coverage at noon, which may be due in part to cirrus shield spreading, is therefore not fundamentally in disagreement with this hypothesis.

4. MODULATION OF THE CONVECTION BY EASTERLY WAVES

The intraseasonal fluctuations of the tropical convection appear to be mainly at short time scales in relation with synoptic-scale tropospheric wave disturbances (Nitta et al., 1985). Over Africa, more than 70% of the interdiurnal variance of the convection occurs in the 1-8 day band (Duvel, 1988). It is then important to understand the interaction between the cloudiness and wave disturbances. This section focuses on the relation between the cloudiness and the African easterly wave disturbance. This relation is obtained by comparing the analysed fields from ECMWF and the cloudiness derived using Meteosat data. The good diurnal sampling (3 hour time step in this study) given by geosynchronous satellites is required because of the strong diurnal cycle of the cloudiness over tropical regions. The use of analysed fields instead of local measurements gives a better basis for General Circulation Model (GCM) validation and for the comparison with satellite measurements. A weak point is that, for most tropical regions of Africa and Atlantic Ocean, the relatively poor amount of data ingested in the analysis is a source of uncertainty. Recent studies of Reed et al. (1987; 1988) show, however, that analysed wind fields describe the African wave disturbances over West Africa and adjacent Atlantic Ocean. Results reported in Duvel (1990), comparing ECMWF analysis and satellite data, confirms the ability of the analysis procedure to describe easterly waves, even in data-sparse regions of the Ocean or Sahel.

Composite analysis makes it possible to normalize the wave perturbation in time, an important procedure because the period of African wave disturbances varies from 2.5 to 5.5 days. The aim of the composite analysis is to display the average variation of atmospheric parameters relative to the average wavelength of the wave. In this study, the wave perturbation of these parameters is defined in regard to the perturbation of the meridional wind at 850 mb (V850). The composite method used and results are described in detail in Duvel (1990). We give here only the main results obtained on the relation between the observed cloudiness and the dynamic and thermodynamic fields described by ECMWF analyses. Additional results, on the moisture budget associated to Easterly waves and on the wave modulation of cluster size, also are given in this section 4.

On the average over three summers (83-85), the wave modulation of the cloudiness is a maximum near the coast of West Africa. The phase of the cloudiness relative to the wave varies strongly with the geographical location in response to changes in the mean structure of the atmosphere. To study the causes of these different phases, vertical cross sections of the wave modulation of the atmospheric state were computed for four large areas (fig.1) having nearly homogeneous phases during the summer of 1985. Wave modulation of the IR histograms on the average over each region is reported on Fig. 7a. On this figure, ordinates are linear in IR radiances. Grey levels represent the number of pixels emitting in a given IR radiance interval (0.25 Wm^{-2} sr^{-1}) expressed as a percentage of the total number of pixels of the region. In order to have a better basis of comparison with vertical cross sections of atmospheric parameters, the IR scale of the wave histogram evolution is converted into pressure scale. This pressure scale is computed for each region using the LOWTRAN radiative transfer model (Kneizys et al., 1983) with the mean

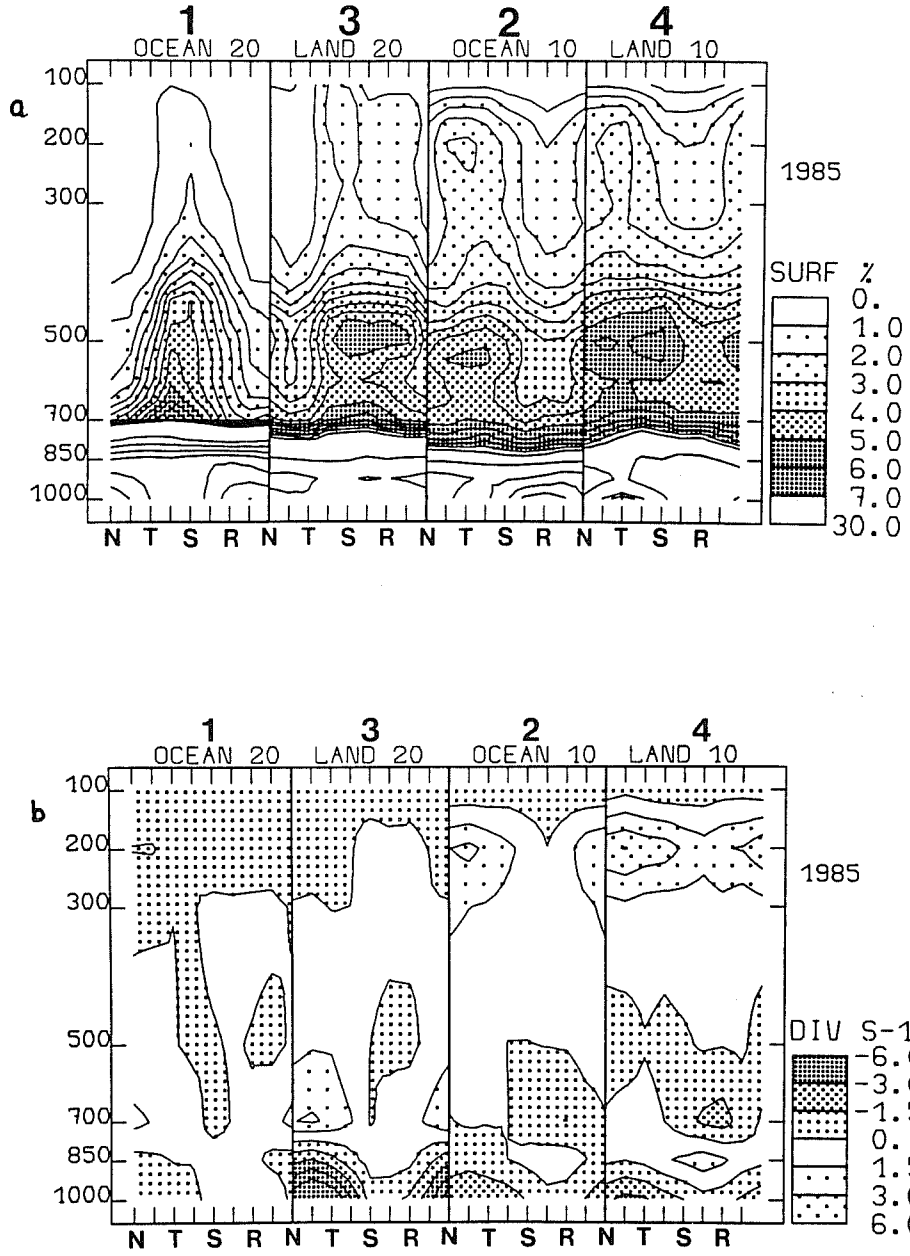

Fig.7: (a) Wave modulation of the IR histograms for summer 1985. Abscissas are categories (N for maximum northerly wind; T for the trough; S for maximum southerly wind; R for the ridge). Ordinates are pressure levels corresponding to IR radiances and computed using a radiative transfer model (see text). The percentage of surface is multiplied by a factor 2 for regions 1 and 3. (b) Vertical cross-sections of the wave modulation of the divergence ($10^{-6}s^{-1}$).

temperature and water vapor profiles for summer 1985. In this computation we assume that cloud tops emit as a black body at the temperature of their pressure level. White areas under 700 mb must be considered with care since these levels may be contaminated by surface emission especially over land. Vertical cross section of the wave modulation of the divergence is reported in fig. 7b.

There are only small differences between wave characteristics of land and oceanic portions of the active ITCZ around 7.5° N. For these regions, convective activity is maximum just ahead of the trough where there is an increase in low-level convergence and 200 mb divergence. Results obtained suggest that the increase in low-level convergence and high-level divergence observed ahead of the trough is mainly a result of the latent heat release by convection. Over oceanic regions around 7.5° N, the general behavior of the wave perturbation of the atmospheric state is in good agreement with results from the GATE ship array and the observed cloud modulation. The main difference with results obtained during GATE is a smaller amplitude of the fluctuations in the present study. This difference may be explained by the GATE studies focusing on a shorter period of especially strong wave amplitude and by smoothing of meteorological fields produced by the ECMWF analysis method (Reed et al, 1988). Over ocean, practically the only wind data come from satellite cloud tracking. The wave is thus often very dependent on the forecast which tends to weaken its amplitude (Laurent et al., 1989). This may also in part explain the weak wave amplitude relative to GATE results.

Over Saharo-Sahelian regions, shallow dry convection dominates ahead of the trough under highly cloud-suppressed conditions (fig.7) consistent with subsidence given by the analysis above 500 mb. The corresponding low-level convergence, therefore, cannot be attributed to deep convection. This enhanced low- level convergence may be due in part (i) to boundary layer surface friction which should be stronger than for regions further south because of the stronger cyclonic vorticity near the surface (ii) to conservation of the potential vorticity at the jet-level described by Mass (1979). It is, however, certainly also related to the southward migration of the low-level convergence zone between the monsoon flow and the northwesterly Harmattan, this zone being on the average located around 20° N. Results suggest that, ahead of the trough, the relative humidity is not large enough to allow the release of conditional instability by the increase of low-level convergence. For Saharo-Sahelian regions, deep convection has a primary maximum on the phase of maximum low-level southerly wind and a secondary maximum east of the ridge. The enhancement of deep convection appears to be primarily related to the increase of low-level moisture content due to the strengthening of the monsoon flow. The effect of the increased convection on the divergence pattern (fig.7b) is weaker than for regions further south because of the relatively weaker convective activity. The feedback of the convection on the wave over these regions is quite small and not positive because the increased cyclonic vorticity induced by the deep convection does not occur on the trough.

The modulation of the high cloud cover (> 13 km) structure by easterly waves is summarized in fig 8 for land and oceanic ITCZ regions (regions 2 and 4 which present a similar response to the wave). Both the high cloud cover and the number of clusters have maxima in the trough and minima in the ridge (fig.8c and 8d). Clusters at all sizes undergo similar modulation (fig.8a), showing that the reinforcement of the convection in the trough is not due only to large clusters. In the other 3 phases of the wave, the cluster size distribution is similar, except the relatively small surface covered by large clusters (around 100 km) in the vicinity of the ridge. Over Saharo-Sahelian regions, the high cloud

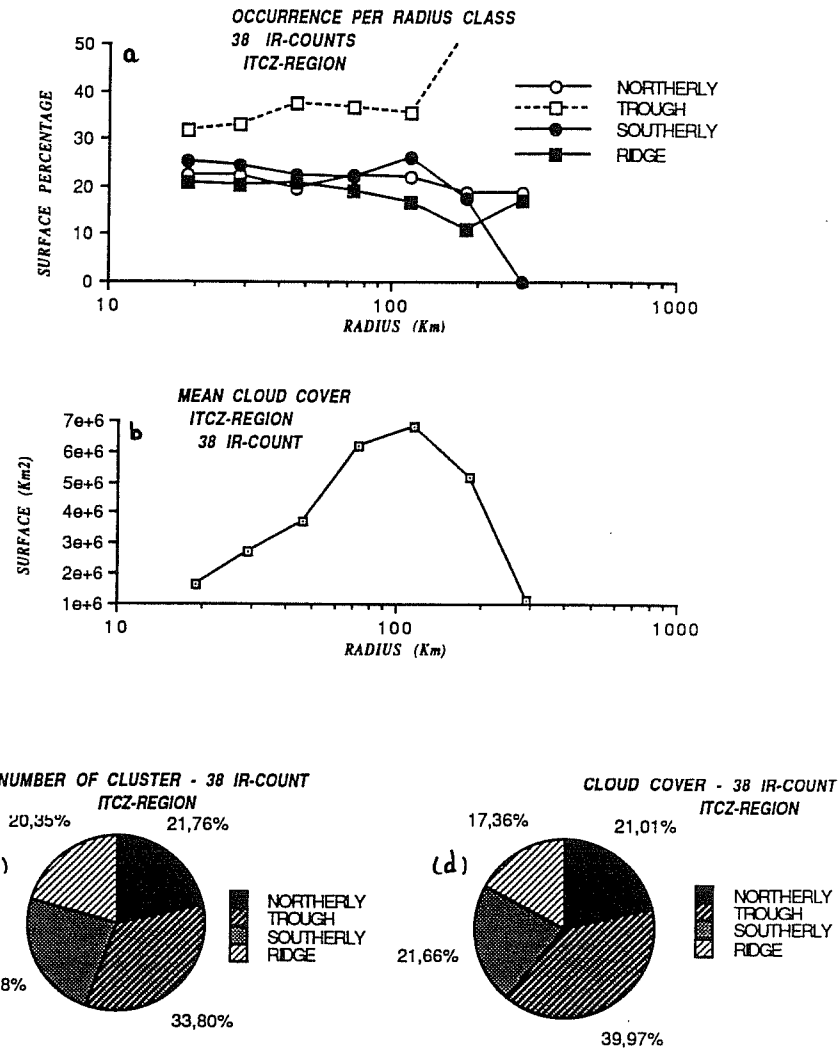

Fig.8 As in fig.5 but for the easterly wave modulation of cluster size over ITCZ regions 2 and 4.

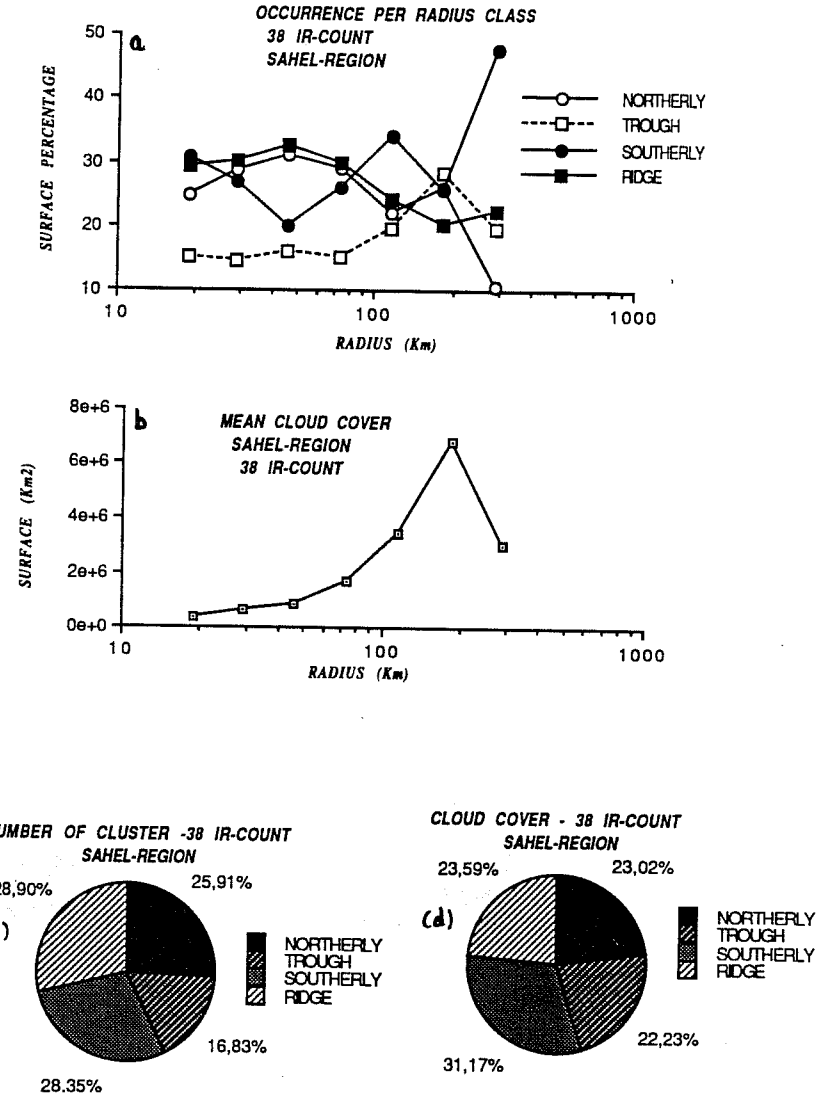

Fig.9: As in fig.5 but for easterly wave modulation of cluster size over Saharo-Sahelian regions (region 3).

cover is maximum in the maximum southerly wind phase (fig.9d), the 3 other phases considered having nearly the same cover. However, the number of clusters presents a sharp minimum in the trough and equal maximum values in the ridge and maximum southerly wind phases (fig.9c). On the opposite to ITCZ regions, the wave alters significantly the cluster size distribution. The wave modulation of the cluster size is however relatively noisy (fig.9a), may be because of the relatively poor mean cloud cover. The maximum cloud cover in the phase of southerly wind seems to be due mainly to large clusters (R>100km), while the large amount of clusters in the ridge is mainly related to smaller clusters (R≈50km). In the trough, the amount of clusters is minimum for nearly all sizes.

Because of the good phase coherence between the observed modulation of the cloudiness and of the atmospheric state described by ECMWF analyses (Duvel,1990), it is possible to make an estimate of the moisture budget. This estimate is a rough one, since absolute values and amplitude of the fluctuations have not been tested and since the vertical resolution (7 pressure levels) and the temporal resolution (12 hours) are coarse. The moisture budget has been initially computed over each of the 2.5° regions and then averaged over the 4 nearly homogeneous regions defined previously. In the calculation, we consider that secular variations and vertical fluxes above 100 mb are negligible. We consider also that the divergences of liquid water and ice are negligible relative to the water vapor divergence. For each 2.5° region, the moisture budget equation for each category may be written as:

$$g^{-1}\int_{p_t}^{p_b} \frac{\partial q_i}{\partial t}\, dp + g^{-1}\int_{p_t}^{p_b} \nabla.(q_i v_i)\, dp = (E_o - P_o)_i \qquad (3)$$

where $\mathbf{v}$ is the horizontal wind (u,v), q the specific humidity, E_o the evaporation rate, P_o the precipitation rate and g the acceleration of gravity. p_b and p_t are respectively the pressure at the bottom and the top of the layer and i refers to the category. The first term to the left is the storage or accumulation rate for each category (A_q^i) and the second term is the net flux moisture divergence for each category (D_q^i). Considering the whole oscillation, this equation may be rewritten as:

$$g^{-1}\int_{p_t}^{p_b} \nabla.(\overline{q}\,\overline{v})\, dp + g^{-1}\int_{p_t}^{p_b} \overline{\nabla.(q_i' v_i')}\, dp = E_o - P_o \qquad (4)$$

where the overbar represents a time average over the whole oscillation (i.e. a summation over the 8 categories NTSR and intermediates). The prime represents a deviation from the time average ($q_i = \overline{q} + q_i'$). The first term represents the mean moisture flux divergence (D_q) and the second term the wave moisture flux divergence D_q^w.

In order to analyse the origin of the water vapor, the moisture flux across the 4 sides of a typical 2.5° region belonging to each large region has been computed for each level and each category. This flux is expressed as:

$$F_i(p_n) = -g^{-1}\int_0^L \int_{p_n}^{p_{n+1}} q_i u_i\, dp\, dl \qquad (5)$$

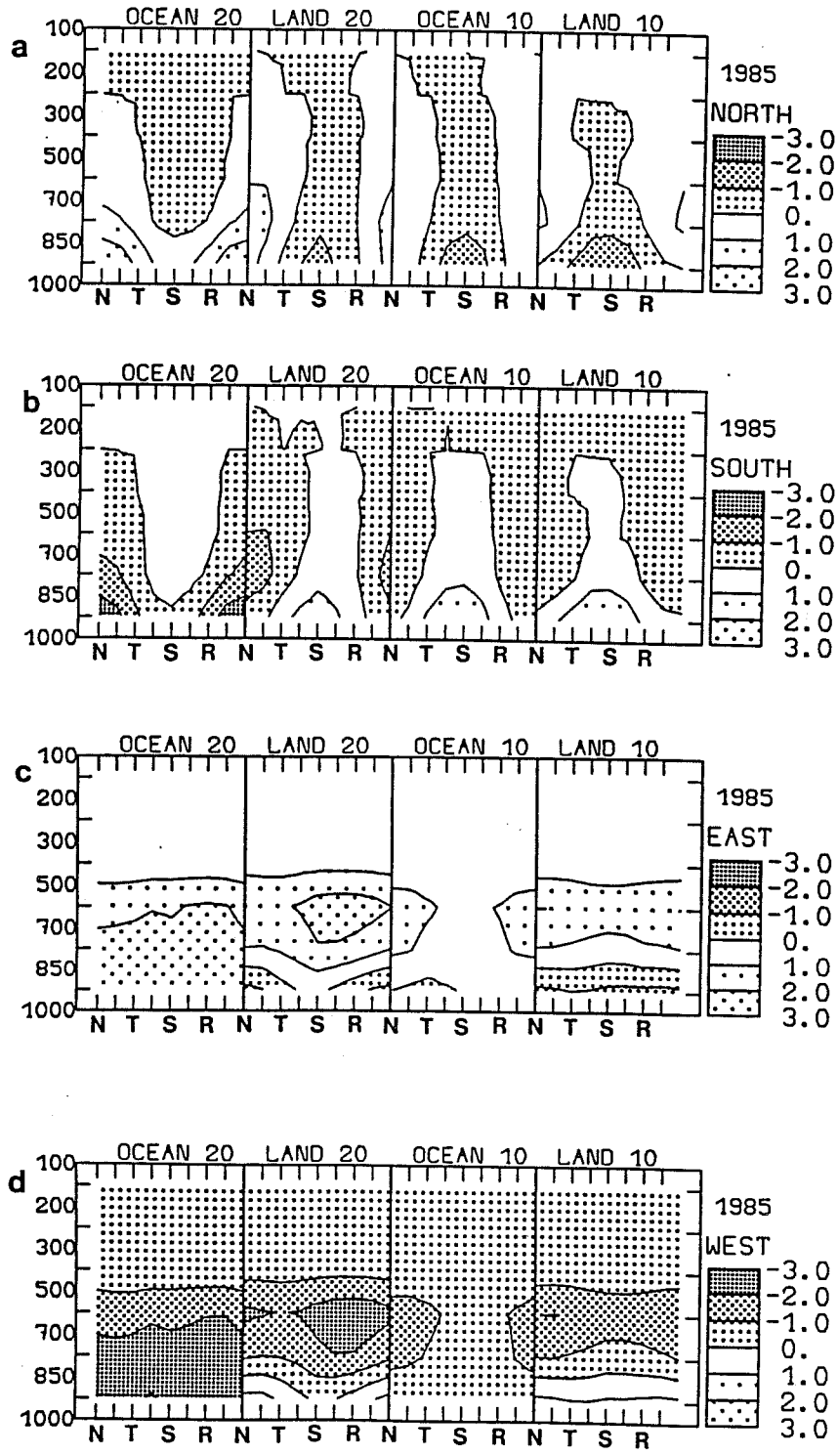

Fig.10: Vertical cross-section of the wave modulation of the moisture flux across the 4 sides of a mean 2.5°x 2.5° area belonging to each large region 1-4 (10^7 kg s^{-1}/2.5°). (a) North side; (b) South side; (c) East side; (d) West side. Fluxes are positive for moisture inflow.

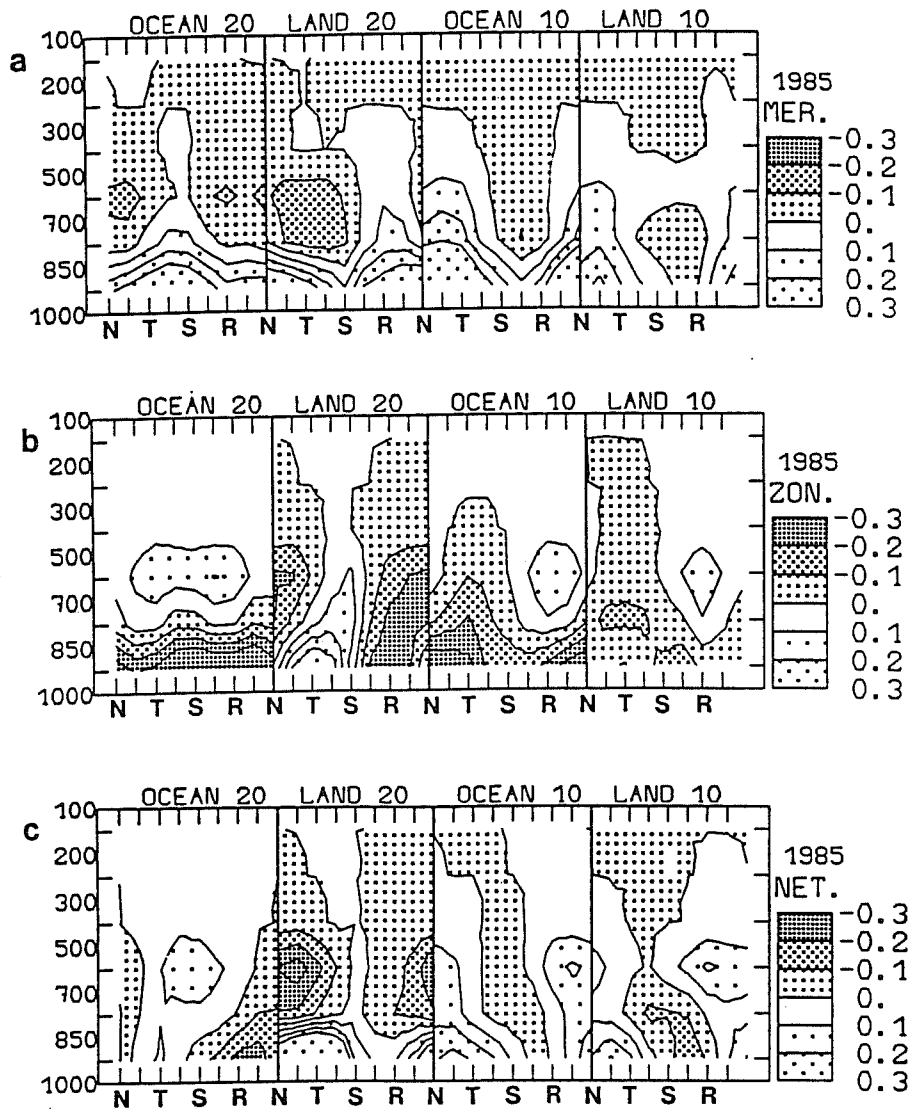

Fig.11 : Vertical cross-section of the wave modulation of the moisture convergence on the average over the 27 2.5°x 2.5° areas belonging to each large region 1-4. (a) meridional convergence; (b) zonal convergence; (c) net convergence (10^7 kg s^{-1}/2.5°).

where p_n and p_{n+1} are 2 adjacent available pressure levels, u is the wind normal to the section, L the total length of the section (2.5°), q the specific humidity on the section and i refers to the category. Results reported in figures 10 and 11 are flux and net flux integrated between 2 adjacent pressure levels. Humidity Fluxes (HF) and their convergences, averaged vertically and over the summer, are reported on table 2. All these results must be considered as characteristic of a typical (average) 2.5°x 2.5° region belonging to the larger regions.

a. Oceanic region between 5°N and 10°N (Region 2)

Over region 2, there is on the average a zonal HF divergence lower than the meridional HF convergence (table 2). Mean zonal HF are easterly mainly in relation with the African Easterly Jet (AEJ) and mean meridional HF results mainly from South-easterly trades (fig.10). Compared to results of Thompson et al. (1979), the net HF convergence found in the present study is smaller by roughly a factor 3 considering whole region 2 and by a factor 2 considering only 2.5° regions corresponding to the GATE area. It is difficult to trace the source of this difference which could be attributed to the different sample (20 days in September 1974 instead of 4 months in 1985) or to underestimates by ECMWF analyses related to the lack of moisture data over this region.

TABLE 2. Mean humidity fluxes (mm day^{-1}) across the 4 sides (N,S,E and W) on the average over the 27 2.5°x 2.5° areas belonging to the larger regions 1-4 (inflows positive). Meridional, zonal and net humidity flux convergences are also reported.

Region	Nort h	Sout h	Meri d.	East	West	Zona l	Net
Ocean 20	23.7	-20.2	3.5	82.5	-85.6	-3.1	0.4
Ocean 10	-0.5	6.9	6.4	26.8	-29.7	-2.9	3.5
Land 20	6.4	-3.1	3.3	44.4	-45.7	-1.3	2.0
Land 10	-4.3	7.0	2.7	21.6	-22.5	-0.9	1.8

TABLE 3. Wave modulation of the accumulation rate (A_q), the moisture divergence (D_q+D_q^w) and the difference between evaporation and precipitation E_o-P_o (expressed in mm day^{-1}).

Cat.		N	3	T	5	S	7	R	1	M
1	D^i_q	3.4	-1.0	-4.4	-4.0	-2.8	-0.8	2.0	4.3	-0.4
Ocean	A^i_q	-2.6	2.2	3.8	2.5	0.7	-0.4	-2.0	-4.2	0.0
20°N	Eo-Po	0.8	1.2	-0.6	-1.5	-2.1	-1.2	0.0	0.1	-0.4
2	D^i_q	-7.3	-7.0	-4.1	-1.4	0.5	0.5	-3.0	-6.2	-3.5
Ocean	A^i_q	2.6	1.5	-0.5	-1.7	-2.5	-2.4	0.5	2.5	0.0
10°N	Eo-Po	-4.7	-5.5	-4.6	-3.1	-2.0	-1.9	-2.5	-3.7	-3.5
3	D^i_q	-0.2	-2.5	-6.0	-5.8	-2.7	0.0	1.0	0.5	-2.0
Land	A^i_q	-3.0	-0.5	2.4	4.5	1.5	-1.4	-1.0	-2.5	0.0
20°N	Eo-Po	-3.2	-3.0	-3.6	-1.3	-1.2	-1.4	0.0	-2.0	-2.0
4	D^i_q	-5.1	-5.1	-2.3	1.2	1.2	1.7	-2.0	-4.1	-1.8
Land	A^i_q	1.9	1.3	-0.5	-1.8	-1.7	-1.1	0.3	1.6	0.0
10°N	Eo-Po	-3.2	-3.8	-2.8	-0.6	-0.5	0.6	-1.7	-2.5	-1.8

The phase of D_q^i (Table 3) is in good agreement with the results of Thompson et al (1979) who found a maximum HF convergence ahead of the trough and slight divergence near the ridge. The storage rate A_q^i, maximum in the northerly wind phase, also is in good agreement with the results of Thompson et al both in phase and amplitude. The

modulation of the resulting term E_O-P_O is in close agreement with the phase of the high cloudiness (fig.7). Assuming that the modulation of the cloudiness is directly related to the rainfall modulation and that the wave modulation of the evaporation is weak, this tends to show that ECMWF analyses should be, at least qualitatively, able to describe the wave modulation of rainfall. Results of Thompson et al. show effectively a small modulation of the evaporation. Over the GATE region in summer 1974, 3/4 of the precipitation was supplied by moisture inflow from surrounding regions and 1/4 by local evaporation. In addition, modulation of the moisture amount is nearly in phase with the modulation of the cloud amount (table 3). The moisture support for the increased convection ahead of the trough results then more from the direct HF convergence than from local evaporation and moisture storage during preceding phase of the wave.

Ahead of the trough, ECMWF analyses describe a strong humidity exchange with surrounding regions with zonal HF divergence and meridional HF convergence (fig 11). The direct moisture support results from meridional convergence of a northerly HF at low and mid-level (fig.10). As stated by Reed and Recker (1971) or earlier by Riehl and Malkus (1958), only air from the boundary layer has sufficient buoyancy to reach the upper level divergent region. However, both updraft and downdraft (Nitta, 1977; Jonhson, 1978) take place in strong convective events showing that a portion of the moisture which converge aloft enters the boundary layer rather than the rising cloud mass (Reed and Recker, 1971). Thus, the net HF convergence at mid-level (fig.11) between the ridge and the trough also certainly contributes to increase deep convective activity. Between the trough and the ridge, the moisture content decreases and HF become divergent on the mean over the summer (table 3). This does not exclude convergence situation during these phases of the wave where we find some high cloudiness.

b. Land region between 5°N and 10°N (Region 4)

Over region 4, zonal HF is slightly divergent (table 2). The strong easterly HF related to the AEJ (fig.10) is in good agreement with results obtained by Cadet and Nnoli (1987) for summer 1979. The weak net convergence, resulting mainly from meridional HF convergence of the monsoon flow, is also in good agreement with these results. This shows nearly balanced evaporation and rainfall.

Compared to region 2, there are only small differences in HF and cloud cover (fig.7) modulations. One of these differences is that the maximum meridional convergence ahead of the trough is related to a nearly equal contribution of a southerly monsoon inflow and a northerly inflow above 850 mb. In fact, nearly half of the moisture supply ahead of the trough is from Sahelian regions at mid-levels (AEJ). As for region 2, downdrafts certainly transport a part of this moisture to the boundary layer giving then an effective moisture supply for the increased convection ahead of the trough. In addition, fig.11 shows that HF is convergent on the average at the level of the AEJ (mainly a meridional convergence). This shows that ECMWF analyses describe an effective moisture supply from the AEJ over region 4 during summer 1985. The main difference in the cloud modulation between region 2 and region 4 is the increased amount of mid-level cloud around cat.6 for land regions. The enhanced monsoon flow in cat.6 corresponds however to net divergence at low levels; this monsoon flow converges northward over Sahelian regions.

c. Land region between 15°N and 20°N (Region 3)

From table 2, one could derive that the moisture support of region 3 is mainly due to the convergence of a northerly HF. Examination of the vertical structure reveals however a convergence of the southerly monsoon flow and divergence of a strong northerly HF related to the slight southward orientation of the AEJ.

There is maximum HF convergence on the trough and slight HF divergence on the ridge (Table 3). The storage rate is strongly modulated by the wave and the term E_o-P_o has 3 minima in categories 2, 4 and 7. This phase does not agree with the phase of the cloudiness which is maximum in categories 5-6 and 1. Examination of the cloud behavior shows strong gradients ahead of the trough suggesting that a part of this disagreement may be related to the computation of the storage rate on the basis of centered finite differences with a large time step. This discrepancy may be also related to the fact that the cloudiness is mainly concentrated to the south of region 3.

Contrary to convectively active regions 2 and 4, the increased cloudiness is not associated with meridional HF convergence and zonal HF divergence. For region 3, the increased convection east of the trough corresponds to low-level zonal convergence of a westerly HF and to mid- level zonal convergence of the AEJ (fig 10 and 11). For these categories, the low-level meridional HF convergence is minimum. The maximum meridional HF convergence occurs east of the ridge corresponding then to the secondary convective maximum. Net HF are however divergent for these categories suggesting that a part of the moisture support is from evaporation and storage. Note that on the contrary with regions further south, the AEJ is a moisture sink over Saharo-Sahelian regions (fig.11c).

For regions 3, D_q^W is slightly positive (0.3 mm day^{-1}) suggesting that the wave leads to increased evaporation compared to precipitation. This means a net loss of precipitation only if the wave reduces or does not change the mean evaporation. Examination of the wave humidity fluxes ($q_i'u_i'$) reveals that the net wave zonal flux divergence is nearly zero for both regions. This divergence is then only a result of a net wave meridional flux divergence related to an unbalanced northward wave humidity flux mainly at low levels. For regions 2 and 4, both wave meridional and zonal flux divergences are nearly zero at all levels. The ECMWF analyses are perhaps not sufficiently precise for correct estimate of D_q^W, the consistency of the results suggests however that this tendency is real.

5. CENTRAL AFRICAN STANDING OSCILLATION

Mainly due to the lack of data, there is to our knowledge no evidence of a synoptic scale organisation of the convection over Central Africa. Especially over these regions poorly covered by conventional meteorological stations, only satellite measurements are able to give spatially and temporally coherent information needed to study fluctuations of the convection. Over Central Africa, as over West Africa, more than 70% of the interdiurnal variance of the convection occurs in the 1-8 day band (Duvel, 1988). In August-September, map of the spectral amplitude of the modulation of the IR signal in the [2.8-5.1] day band (fig.12) exhibits two main maxima located around (7.5°N-27.5°E) and (2.5°N-20°E), corresponding respectively to regions located northeast and southwest of a mountain ridge (fig.1). These locations remain the same during the 3 summers (83-85) and are located over lowlands of Southern Sudan and Northern Congo. The average power spectra of the cloud

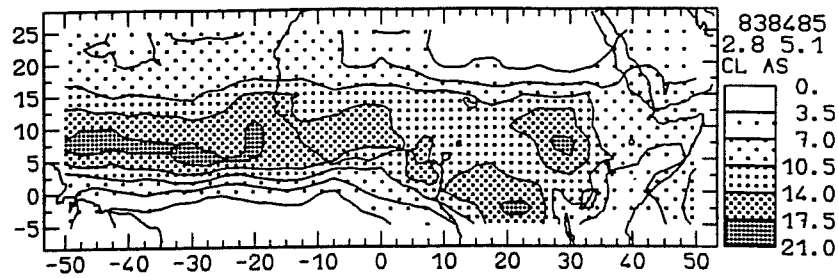

Fig.12: Square root of the variance of the cloud (CL) fluctuations in the 2.8-5.1 day band (a) June and July 1983-85 (b) August and September 1983-85.

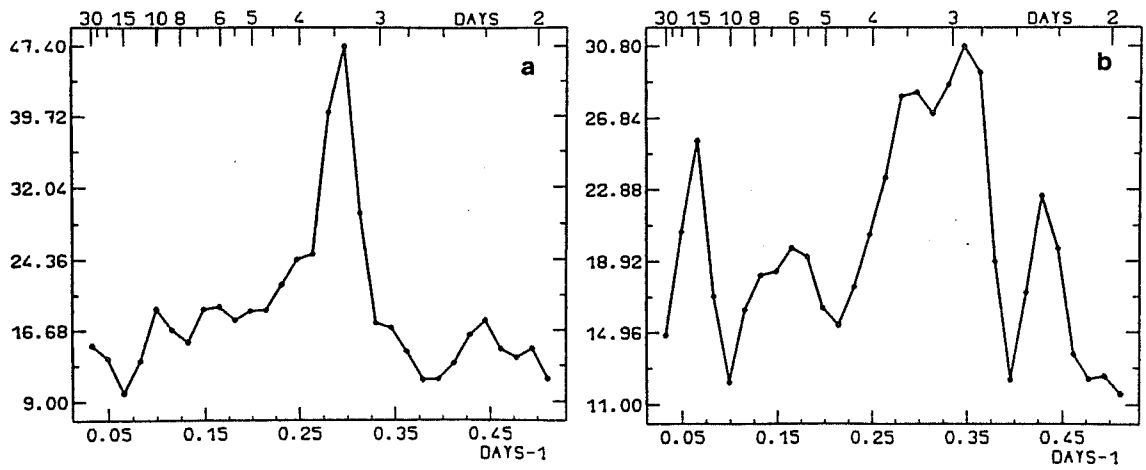

Fig.13: Power spectrum of the the cloud (CL) fluctuations for August and September 1983-85 (a) Region of Southern Sudan (region A) (b) Region of Northern Congo (region B).

(CL) fluctuations over these 3 August-September periods for the two large regions defined on figure 14a exhibit large variance peaks around 3-4 days (fig.13). These maxima are then not related to red noise but to a relatively stable quasi-periodic feature governing the cloud activity over these regions. In order to study the nature of these quasi-periodic fluctuations we use complex EOF analysis described by Wallace and Dickinson (1972) and Horel (1984).

Complex EOF analysis is made here by computing the mean cross- spectrum matrix over 6 AS period (83-88) and for the spectral band [K1, K2] corresponding to periods between 2.9 and 5.5 days. Each element of the matrix is:

$$m(x,y)=\frac{1}{6}\sum_{a=1}^{6}\sum_{k=K_1}^{K_2} c_x^a(k)c_y^{a*}(k) \qquad (6)$$

where $c_x^a(k)$ is the complex Fourier coefficient of the CL time series for year a, region x and harmonic k. Considering N regions, we obtain a N x N hermitian matrix from which we compute N real eigenvalues k_n and complex eigenvectors $Z_n(x)$ using the EVEHF subroutine of the IMSL. In this study, we use only the 2 first principal components corresponding to the largest eigenvalues. The spatial distribution of the amplitude of the first principal component is given by the square root of:

$$a_1(x) = k_1 \left| Z_1(x) \right|^2 \qquad (7)$$

The relative phase between the regions is given by:

$$\Phi_1(x) = \arg\,[Z_1(x)] \qquad (8)$$

The normalized power spectrum of the first principal component for year a is given by:

$$S_1^a(k)= \left| s_1^a(k) \right|^2 \qquad (9)$$

where

$$s_1^a(k) = \sum_{x=1}^{N} \frac{c_x^a\, Z_1(x)}{\lambda^{1/2}} \qquad (10)$$

The temporal evolution of the amplitude is given by the square root of the module of the inverse Fourier transform of the spectrum $s_1^a(k)$.

The first complex principal component (fig.14) describes a standing oscillation between Northern Congo (region B) and Southern Sudan (region A). This first component represents more than 26% of the variance of the whole geographical domain of fig.14 and for the spectral band considered. The 2 centers of this oscillation are located northeast and southwest of the small mountain ridge (fig.1) over which there is the maximum of high cloud coverage on the average over the 6 summers. On these 2 centers, the 1st EOF

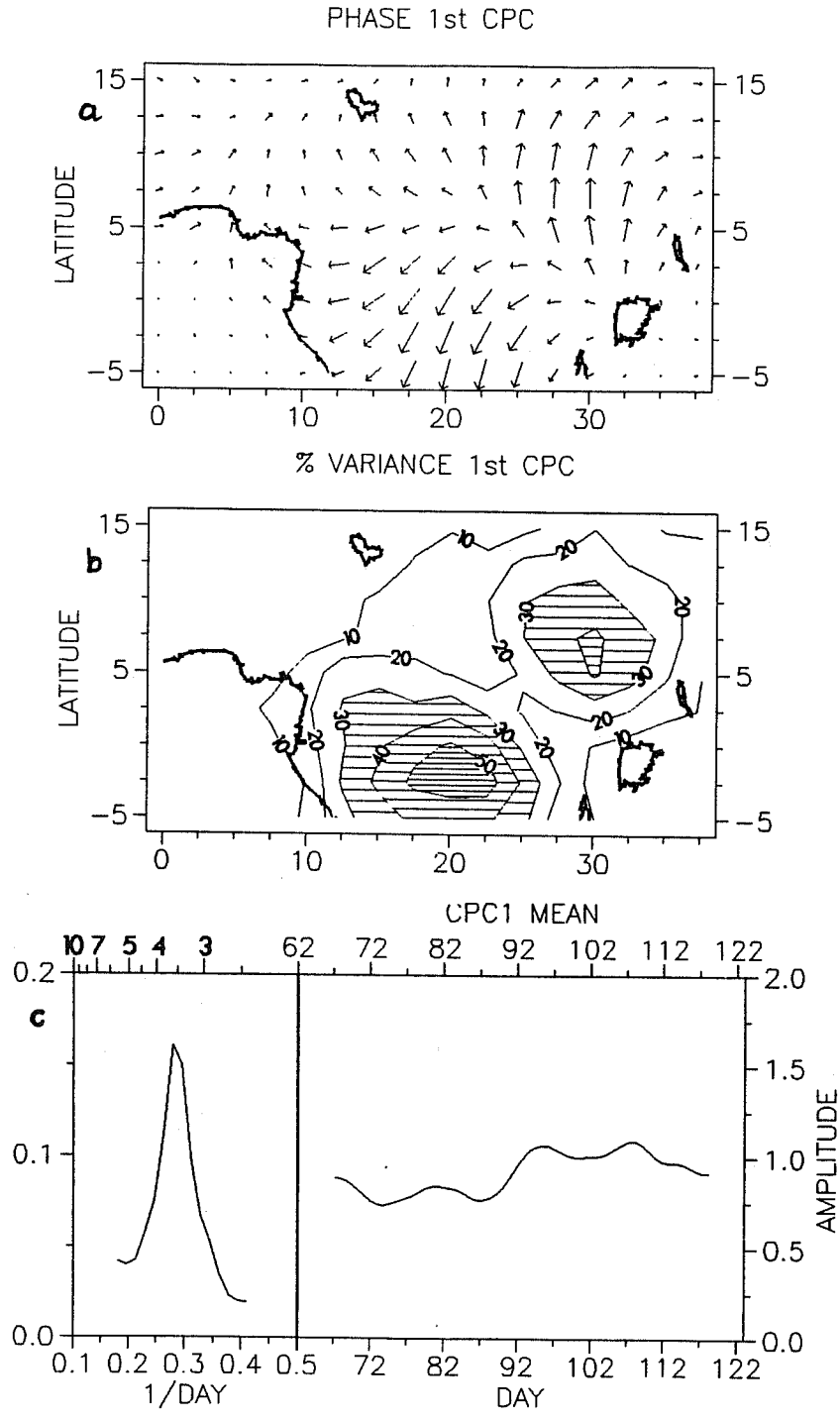

Fig.14: (a) Phase (eq.8) of the first complex EOF of the cloud (CL) fluctuation in the 2.9-5.5 day band. (b) Amplitude of the first complex EOF expressed as a percentage of the total inter-diurnal variance. (c) Mean power spectrum (eq.9) and temporal evolution (day 62 = August 1) of the 1st EOF.

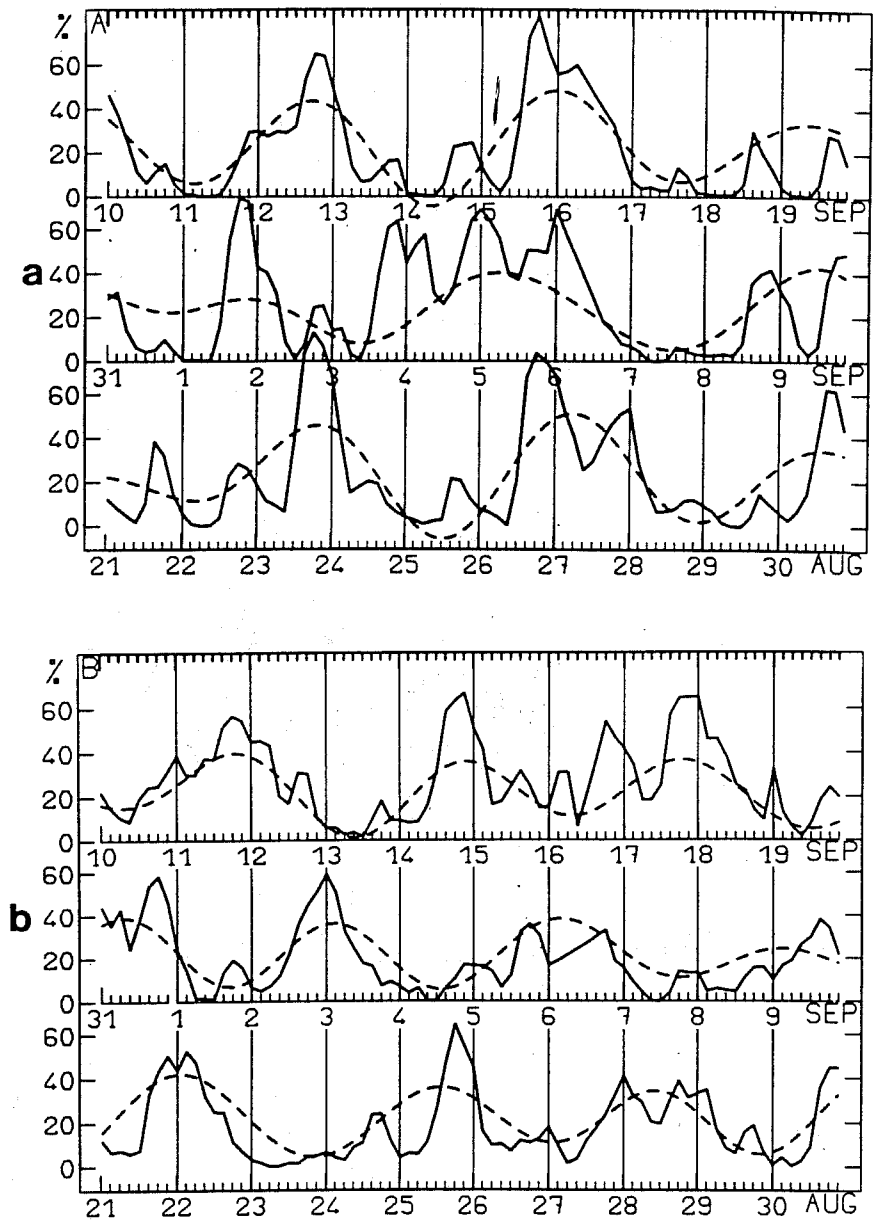

Fig.15: (solid line) Temporal evolution (21 August-19 September 1984) of the high cloud cover (EBBT<253K) (dashed) Filtered signal around 3.5 days (a) Region A (b) Region B.

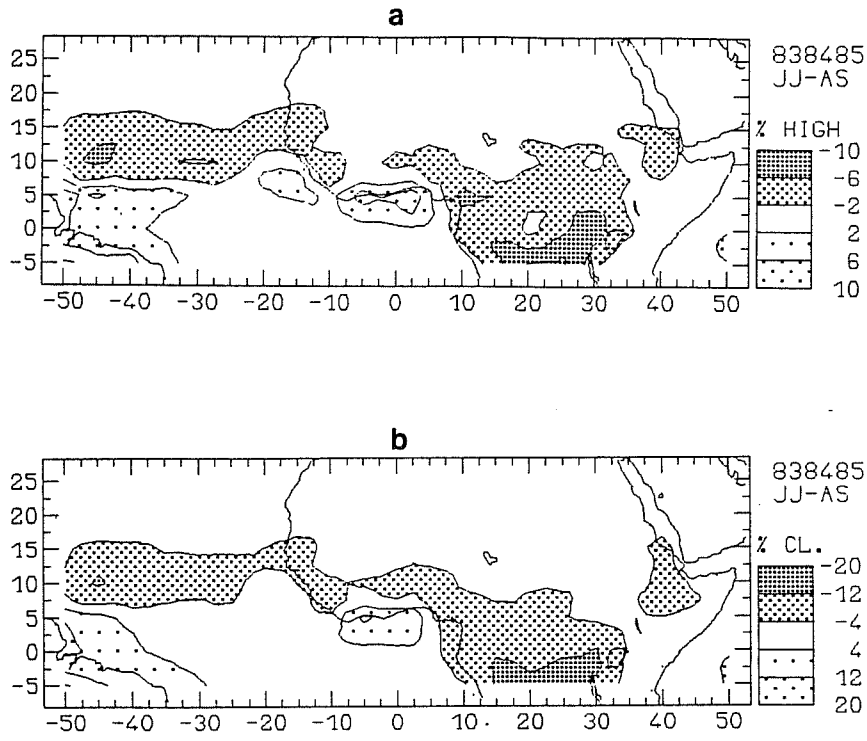

Fig. 16: Difference between June-July and August-September in the mean cloud cover (83-85)
(a) High cloudiness (EBBT<253K) (b) High and mid-level cloudiness (EBBT<476.5K)

represents more than 40% of the total inter-diurnal variance. The northeast regions are located close to this maximum and the oscillation appears then as a fluctuation of the northeastward extent of this maximum. The southwest regions are however farther from this ridge and are more centered on the basin of Northern Congo. Power spectra of this first principal component (fig 14c) have a peak in the 3-4 day band with a good interannual reproducibility (not shown). The temporal evolution of the amplitude of the standing oscillation (1st component) on the average over the 6 AS periods does not show any significant trend.

Superposition of the filtered (around 3.5 days) and the raw HI signals for AS 1984 shows that the fluctuations of the high cloudiness over regions A and B are highly related to the diurnal variation and to the oscillation around 3-4 days (fig.15). The result is equivalent for the 2 other AS periods 83 and 85. This figure shows a strong interaction between the diurnal variation and the oscillation giving amplitude greater that 60% of the effective high cloud coverage. In fact, the temporal evolution exhibits clearly that a strong cloud development cannot generally appear over both regions the same day. There is then an inhibiting effect of one region on the other appearing mostly in the AS period.

The mechanism of this standing oscillation may be tentatively explained by quasi-periodic fluctuations of the convection over northern Congo (region B) generated by feedbacks between hydrological processes and the basic forcing of the convection, i.e. the radiative surface heating. This is similar to the hypothesis of Webster and Chou (1980) to explain quasi-periodic breaks of the Indian monsoon. Over region B, convective development at large scale gives a stabilisation of the temperature profiles and a cooling of the surface (rain and reduced solar heating) which inhibits the convection the following days (2 to 3 days). During these days, temperature profiles become convectively (conditionally) unstable and the surface warms up. This mechanism may explain the standing oscillation and 2 points support this hypothesis :

1 - Over region A, the water vapor supply at low levels is mainly from region B. When strong convection develops over region B on a given day, the northeastward moisture flux to region A is weakened and the convection over this region is inhibited. When the convection over region B is reduced, the convection may develop on region A (a part of the moisture being from evaporation over region B).

2 - Over region B, the cloud cover is larger during AS than during JJ (fig.16) in relation with the latitudinal migration of the ITCZ related to the solar declination. This is in agreement with the fact that the standing oscillation is primarily driven by the convection over region B. During June and July, the characteristic time scale of the fluctuation over region A is rather around 5 days.

The development of the standing oscillation is also dependent on the large scale organisation of the convection over both regions. Figure 15 shows such a large scale organisation with a modulation of more than 60% of the high cloud amount HI (cloud top > 8 km) resulting from the superposition of the diurnal variation and the standing oscillation. This large scale organisation may result from the release of Conditional Instability of the Second Kind (CISK), i.e. the development of convective cells over the region increases the large scale low-level convergence which gives in turn more convective development by releasing conditional instability. This feature may be enhanced by the basin structure of both regions A and B. This interpretation is however only tentative and

the full understanding of the standing oscillation needs more theoretical and observational studies.

6. CONCLUDING REMARKS

This study has shown that the wave modulation of the cloudiness, like the diurnal modulation, may be considered to be a climatological characteristic of West Africa and the neighbouring Atlantic ocean. This is also valid over Central Africa where both diurnal variations and modulation generated by a standing oscillation (3-4 days) are well reproducible from one summer to another. The diurnal evolution of infrared histograms shows that, over the whole of Africa and at this 2.5° horizontal scale, the diurnal behavior of the mid-level and high cloudiness is similar with: a maximum development of high convective cloudiness at the end of the afternoon and a maximum development of mid-level cloudiness at sunrise. Over ocean, cloudiness at all levels presents a coherent and reproducible diurnal variation. The cluster size distribution also has a coherent diurnal variation. Over ocean, the diurnal variation of the high cloudiness is mainly due to clusters with radius larger than 100 km. This is an interesting point for a better understanding of the origin of the diurnal variation of the convection over ocean. However, the physical basis of this diurnal variation needs to be addressed. Although complete understanding of oceanic convective activity requires collecting more atmospheric conventional data, the discrimination between convective and non-convective clouds should give interesting additional information. It should be especially interesting to distinguish between the convectively active part of the clusters and the cirrus shield.

A striking result is the strong geographical dependence of the phase of the cloud response to easterly waves. The longitudinal and the latitudinal dependence of the phase of the cloudiness response must then be considered for a correct estimation of the wave characteristics (phase speed, wavelength) on the basis of IR satellite observations alone. That the phase of the cloud modulation by easterly waves should depend on the mean atmospheric state, or climate, of the underlying region, is not surprising, and it also can be an interesting basis of validation of convection and cloud parametrizations in GCMs. For the oceanic part of the active ITCZ, and despite the small amount of moisture data, ECMWF analyses reproduce fairly well the phase of the wave modulation of the different terms of the moisture budget found during GATE. The amplitude of the modulation of the moisture divergence and the mean divergence are however too small. On the contrary, the mean moisture divergence found over West Africa is in agreement with previous results obtained for summer 1979 by Cadet and Nnoli (1987). Over these regions, estimates of humidity flux (HF) convergence reveal that ahead of the trough there is strong humidity exchange with surrounding regions with zonal HF divergence and stronger meridional HF convergence at low and mid- levels. ECMWF analyses also show that, for summer 1985, the AEJ was a humidity source over West Africa.

For the active part of the ITCZ, the organisation of the convection gives a positive feedback on the wave. Recent work (Laurent et al., 1989) has shown that, for the 1985 version of the model, the amplitude of the wave progressively decays in the ECMWF forecasts over West Africa. The wave amplitude is reduced by a factor 2 in the 2-day forecast and becomes nearly zero after 4 days. This decay of the wave in the forecast may well be caused in part by under-evaluation of the feedback of the deep convection. Further studies are then needed in order to quantify this feedback and it will be interesting to make

the same kind of analysis with new versions of the ECMWF model. Analyses of quasi-periodic features, such as the central African standing oscillation, should also be an interesting approach of the validation of the parametrization of the tropical deep convection.

Acknowledgments. This work was supported in part by the Centre National d'Etudes Spatiales. The Meteosat B2 data sets are prepared by the European Space Operations Centre of the European Space Agency, as part of the International Satellite Cloud Climatology Project of the World Climate Research Programme. Meteorological fields are prepared by the European Center for Medium Range Weather Forecast. L.A. Toledo Machado is preparing a PhD thesis under a scholarship of the Instituto de Atividales Espaciais (Centro Técnico Aeroespacial. Saõ Paulo. Brazil.).

REFERENCES

Albright , M.D., E.E. Recker, R.J. Reed and R. Dang, 1985 : The diurnal variation of deep convection and inferred precipitation in the central tropical Pacific during January-February 1979. *Mon. Wea. Rev.*, **113**, 1663-1680.

Albright, M.D., D.R. Mock, E.E. Recker, and R.J. Reed, 1981 : A diagnostic study of the diurnal rainfall variation in the GATE B-scale area. *J. Atmos. Sci.*, **38**, 1429-1445.

Augustine, J.A., 1984 : The diurnal variation of large-scale inferred rainfall over the tropical Pacific Ocean during August 1979. *Mon. Wea. Rev.*, **112**, 1745-1751.

Bengtsson, L., 1985 : Medium range forecasting at the ECMWF. *Advances in geophysics*, **28**, part. B, 3-54.

Cadet , D.L. and N.O. Nnoli, 1987 : Water vapour transport over Africa and the Atlantic Ocean during summer 1979. *Q. J. R. Meteorol. Soc.*, **113**, 581-602.

Duvel, J.P., and R.S. Kandel, 1985 : Regional-scale diurnal variations of outgoing infrared radiation observed by Meteosat. *J. Climate Appl. Meteor.*, **24**, 335-349.

Duvel, J.P., 1988 : Analysis of Diurnal, Interdiurnal and Interannual Variations during Northern Hemisphere Summers Using Meteosat Infrared Channels. *J. Climate*, **1**, 471-484.

Duvel, J.P., 1989 : Convection over tropical Africa and Atlantic Ocean during northern summer. Part I: Interannual and diurnal variations. *Mon. Wea. Rev.*, **117**, 2782-2799.

Duvel, J.P., 1990 : Convection over tropical Africa and Atlantic Ocean during northern summer. Part II: Modulation by easterly waves. *Mon. Wea. Rev.*, **118**, 1855-1868.

Gray, W.M., and R. Jacobson, 1977 : Diurnal variation of deep cumulus convection. Mon. Wea. Rev., 105, 1171-1188. Gruber, A, 1976 : An estimate of the daily variation of cloudiness over the GATE A/B area. *Mon. Wea. Rev.*, **104**, 1036-1039.

Horel, J.D., 1984 : Complex principal component analysis-theory and examples. *J. Climate Appl. Meteor.*, **23**, 1660-1673.

Johnson, R.H., 1978 : Cumulus transports in a tropical wave composite for phase III of GATE. *J. Atmos. Sci.*, **35**, 484-494.

Jones M., and J. Morgan, 1981 : Adjustment of Meteosat-1 radiometer response by ground processing. *ESA J.*, **5**, 305-320.

Kneizys, F.X., E.P. Shettle, W.O. Gallery, J.H. Chetwynd Jr., L.W. Abreu, J.E.A. Selby, S.A. Clough, and R.W. Fenn, 1983 : Atmospheric Transmittance/ Radiance / Computer

Code Lowtran6, AFGL-TR-83-0187, Environmental Res. Paper No. 846, 200 pp., (Available from, AFGL (OPI), Hanscom AFB, MA01731, USA).

Laurent, H., A. Viltard and P. de Felice, 1989 : Performance evaluation and local adaptation of the ECMWF system forecasts over northern Africa for summer 1985. *Mon. Wea. Rev.*, **117**, 1999-2009.

Lorenc, A.C., 1981 : A global three-dimensional multivariate statistical interpolation scheme. *Mon. Wea. Rev.*, **109**, 701-721.

Mass, C., 1979 : A linear primitive equation model of African wave disturbances. *J. Atmos. Sci.*, **36**, 2075-2092.

Murakami, M. , 1979 : Large-scale aspects of deep convective activity over the GATE area. *Mon. Wea. Rev.*, **107**, 994-1013.

Nitta, T., 1977 : Response of cumulus updraft and doowndraft to GATE A/B-scale motion systems. *J. Atmos. Sci.*, **34**, 1163-1186.

Nitta, T. and Y. Takayabu, 1985 : Global analysis of the lower tropospheric disturbances in the Tropics during Northern Summer of the FGGE year. Part II: Regional characteristics of the disturbances. *Pageoph*, **123**, 272-292.

Reed, R.J, A. Hollingsworth, W.A. Heckley and F. Delsol, 1988 : An evaluation of the performance of the ECMWF operational forecasting system in analysing and forecasting tropical easterly waves disturbances over Africa and the tropical Atlantic. *Mon. Wea. Rev.*, **116**, 824-865.

Reed, R.J. and E.E. Recker, 1971 : Structure and properties of synoptic- scale wave disturbances in the Equatorial Western Pacific. *J. Atmos. Sci.*, **28**, 1117-1133.

Riehl, H. and J.S. Malkus, 1958 : On the heat balance in the Equatorial trough zone. *Geophysica*, **6**, 503-538.

Thompson, R.M., Jr., S.W. Payne, E.E. Recker and R.J. Reed, 1979 : Structure and properties of synoptic-scale wave disturbances in the Intertropical Convergence Zone of the Eastern Atlantic. *J. Atmos. Sci.*, **36**, 53-72.

Wallace J.M. and R.E. Dickinson, 1972 : Empirical orthogonal representation of a time series in the frequency domain. Part I : Theoretical considerations. *J. Appl. Meteor.*, **11**, 887-892.

Webster, P.J., and L.C. Chou, 1980 : Low-frequency transitions of a simple monsoon system. *J. Atmos. Sci*, **37**, 368-382.

Welch, R.M., S.K. Sengupta and K.S. Kuo, 1988: Marine stratocumulus cloud fields off the coast of southern California observed using Landsat imagery. Part II: Textural analysis. *J. Appl. Meteor.* , **27**, 363-378.

Wielicki, B.A., and R.M. Welch, 1986: Cumulus cloud field properties derived using Landsat digital data. *J. Climate Appl. Meteor.*, **25**, 261-276.

Wilson, C.A. and J.F.B. Mitchell, 1986 : Diurnal variation and cloud in a general circulation model. *Quart. J. Roy. Meteor. Soc.*, **112**, 347-369.